Onconase, is able to inhibit protein synthesis in mammalian cells and has been used as a protein drug. When it was added to the culture media of H9 cells persistently infected with HIV-1, HIV-1 replication was inhibited without blocking cell growth, as degradations of 18S and 28S rRNAs and cellular mRNAs were prevented (Saxena *et al.*, 1996). MazF induction in mammalian cells has shown to cause apoptotic cell death as a result of degradation of cellular mRNAs (Shimazu *et al.*, 2007). However, in the present study, MazF expression induced by HIV-1 Tat appears to be maintained at very low levels, just enough to cleave HIV-1 RNA but not cellular mRNAs, so that cells were able to grow normally. MazF expression may be autoregulated in the cell in such a way that when Tat-induced MazF eliminates invading HIV-1 RNA, Tat expression from the HIV-1 provirus is simultaneously stopped, resulting in simultaneous arrest of MazF production to recover normal cellular functions.

Targeting HIV RNA as a therapeutic strategy using antisense RNA (Levine *et al.*, 2006), ribonucleases (Agarwal *et al.*, 2006), and RNA interference (RNAi) technology (Morris and Rossi, 2004) has been attempted. However, the use of antisense RNA and RNAi technology has not been effective as an anti-HIV technology, as HIV can easily circumvent these RNA inhibitors by creating mutations at the target sequence regions (Lee and Rossi, 2004). On the other hand, the present strategy using MazF targets abundant ACA sequences in HIV-1 RNA (>240), so that it is not possible for HIV-1 to escape from MazF attack by mutations. Furthermore, because MazF has no homology to any mammalian ribonucleases, MazF mRNA interferase activity cannot be inhibited by ribonuclease inhibitors existing in mammalian cells.

In summary, the use of MazF appears to be a novel and highly effective tool for anti-HIV gene therapy. It is effectively able to suppress HIV-1 replication, preventing the emergence of mutated HIV-1. Importantly, MazF induction by invading HIV-1 shows little toxicity to host cells while it efficiently suppresses HIV-1 replication. Specific inhibition of HIV-1 replication by MazF without affecting cell growth is the key feature of MazF-based HIV-1 gene therapy. This may be the first step for RNase-based HIV-1 gene therapy with efficacy *in vitro*. The feasibility of the MazF-based *ex vivo* gene therapy may be verified using autologous CD4+ T lymphocytes from HIV-1 patients. To use our *mazF* vector system for gene therapy, its safety has to be critically evaluated and it should not have any negative impacts on T-cell function. For example, it needs to be shown that there is no alteration in the secretion of functionally important cytokines even though it was observed that MazF expression in HIV-infected CD4+ T cells does not inhibit cell growth. We are currently addressing this question.

Acknowledgments

The authors thank Dr. Keith A. Reimann of Harvard Medical School and Dr. Tomoyuki Miura of Kyoto University for providing the SHIV 89.6P. The authors also thank Dr. Koich Inoue of Takara Bio Inc. for his critical reading of the manuscript.

Author Disclosure Statement

No competing financial interests exist.

References

Agarwal, S., Nikolai, B., Yamaguchi, T., Lech, P., and Somia N.V. (2006). Construction and use of retroviral vectors encoding the toxic gene barnase. Mol. Ther. 14, 555–563.

Berkhout, B., Silverman, R.H., and Jeang, K.T. (1989). Tat transactivates the human immunodeficiency virus through a nascent RNA target. Cell 59, 273–282.

Kim, S., Ikeuchi, K., Byrn, R., Groopman, J., and Baltimore, D. (1989). Lack of a negative influence on viral growth by the nef gene of human immunodeficiency virus type 1. Proc. Natl. Acad. Sci. U.S.A. 86, 9544–9548.

Lee, J.T., Yu, S.S., Han, E., Kim, S., and Kim, S. (2004). Engineering the splice acceptor for improved gene expression and viral titer in an MLV-based retroviral vector. Gene Ther. 11, 94–99.

Lee, N.S., and Rossi, J.J. (2004). Control of HIV-1 replication by RNA interference. Virus Res. 102, 53–58.

Levine, B.L., Humeau, L.M., Boyer, J., MacGregor, R.R., Rebello, T., Lu, X., Binder, G.K., Slepushkin, V., Lemiale, F., Mascola, J.R., Bushman, F.D., Dropulic, B., and June, C.H. (2006). Gene transfer in humans using a conditionally replicating lentiviral vector. Proc. Natl. Acad. Sci, U.S.A. 103, 17372–17377.

Miyake, A., Ibuki, K., Enose, Y., Suzuki, H., Horiuchi, R., Motohara, M., Saito, N., Nakasone, T., Honda, M., Watanabe, T., Miura, T., and Hayami, M. (2006). Rapid dissemination of a pathogenic simian/human immunodeficiency virus to systemic organs and active replication in lymphoid tissues following intrarectal infection. J. Gen. Virol. 87, 1311–1320.

Morris, K.V., and Rossi, J.J. (2006). Lentivirus-mediated RNA interference therapy for human immunodeficiency virus type 1 infection. Hum. Gene Ther. 17, 479–486.

Nariya, H., and Inouye, M. (2008). MazF, an mRNA interferase, mediates programmed cell death during multicellular Myxococcus development. Cell 132, 55–66.

Reimann, K.A., Li, J.T., Voss, G., Lekutis, C., Tenner-Racz, K., Racz, P., Lin, W., Montefiori, D.C., Lee-Parritz, D.E., Lu, Y., Collman, R.G., Sodroski, J., and Letvin, N.L. (1996). An env gene derived from a primary human immunodeficiency virus type 1 isolate confers high in vivo replicative capacity to a chimeric simian/human immunodeficiency virus in rhesus monkeys. J. Virol. 70, 3198–3206.

Saxena, S.K., Gravell, M., Wu, Y.N., Mikulski, S.M., Shogen, K., Ardelt, W., and Youle, R.J. (1996). Inhibition of HIV-1 production and selective degradation of viral RNA by an amphibian ribonuclease. J. Biol. Chem. 271, 20783–20788.

Shimazu, T., Degenhardt, K., Nur-E-Kamal, A., Zhang, J., Yoshida, T., Zhang, Y., Mathew, R., White, E., and Inouye, M. (2007). NBK/BIK antagonizes MCL-1 and BCL-XL and activates BAK-mediated apoptosis in response to protein synthesis inhibition. Genes Dev. 21, 929–941.

Silverman, R.H. (2003). Implications for RNase L in prostate cancer biology. Biochemistry 42, 1805–1812.

Verzeletti, S., Bonini, C., Marktel, S., Nobili, N., Ciceri, F., Traversari, C., and Bordignon, C. (1998). Herpes simplex virus thymidine kinase gene transfer for controlled graft-versus-host disease and graft-versus-leukemia: clinical follow-up and improved new vectors. Hum. Gene Ther. 9, 2243–2251.

Yamaguchi, Y., and Inouye, M. (2009). mRNA interferases, sequence-specific endoribonucleases from the toxin-antitoxin systems. Prog. Mol. Biol. Transl. Sci. 85, 467–500.

Yu, S.F., von Rüden, T., Kantoff, P.W., Garber, C., Seiberg, M., Rüther, U., Anderson, W.F., Wagner, E.F., and Gilboa, E.

(1986). Self-inactivating retroviral vectors designed for transfer of whole genes into mammalian cells. Proc. Natl. Acad. Sci. U.S.A. 83, 3194–3198.

Yu, S.S., Han, E., Hong, Y., Lee, J.T., Kim, S., and Kim, S. (2003). Construction of a retroviral vector production system with the minimum possibility of a homologous recombination. Gene Ther. 10, 706–711.

Zhang, Y., Zhang, J., Hoeflich, K.P., Ikura, M., Qing, G., and Inouye, M. (2003). MazF cleaves cellular mRNAs specifically at ACA to block protein synthesis in *Escherichia coli*. Mol. Cell 12, 913–923.

Zhu, L., Zhang, Y., The, J.S., Zhang, J., Connell, N., Rubin, H., and Inouye, M. (2006). Characterization of mRNA interferases from Mycobacterium tuberculosis. J. Biol. Chem. 281, 18638–18643.

Zhu, L., Inoue, K., Yoshizumi, S., Kobayashi, H., Zhang, Y., Ouyang, M., Kato, F., Sugai, M., and Inouye, M. (2009). *Staphylococcus aureus* MazF specifically cleaves a pentad sequence, UACAU, which is unusually abundant in the mRNA for pathogenic adhesive factor SraP. J. Bacteriol. 191, 3248–3255.

Address correspondence to:
Dr. Ikunoshin Kato
Center for Cell and Gene Therapy
Takara Bio Inc.
Seta 3-4-1
Otsu, Shiga
520-2193, Japan

E-mail: ikukatiku@zeus.eonet.ne.jp

Dr. Masayori Inouye
Department of Biochemistry
Robert Wood Johnson Medical School
675 Hoes Lane
Piscataway, NJ 08854, USA

E-mail: inouye@umdnj.edu

Received for publication January 5, 2010;
accepted after revision July 22, 2010.

Published online: July 22, 2010.

第3項　ネフローゼ症候群モデル(ICGNマウス)

ネフローゼ症候群は，重度のタンパク尿，低タンパク血症，高脂血症，浮腫を主たる症状とする疾病で，糸球体疾患を原因とする一次性と他の全身性疾患(紫斑病性腎炎，糖尿病，ループス腎炎など)に起因する二次性とに分類される。本稿で紹介するICR-derived glomerulonephritis(ICGN)マウスは一次性ネフローゼ症候群としての特性を備えた貴重なモデル動物である。

図1　全身性浮腫を呈した雄性ICGNマウス

1. ICGNマウスの由来および原因遺伝子

リンパ節腫大および脾腫を呈する雄性ICRマウスが，1986年に国立感染所研究所(旧国立予防衛生研究所)にて発見された。その個体と正常雌性マウス間の兄妹交配から得られた産仔の中で，浮腫を呈する個体をICGNマウスのF_1として育種が開始され[1]，兄妹交配による近交化を経て病態進行に個体差はあるものの全個体がネフローゼを発症する系統として確立された[2]。ネフローゼ症候群の発症機序は未解明であるが，2006年に細胞接着に関わるtensin2のnt1477-1484(exon18)8塩基の欠失が報告された[3]。Tensin2は正常な腎の糸球体上皮細胞および尿細管に発現していることが分かっているが，腎における機能は不明であり，今後の解析が待たれる。

2. 病　態

生後間もなくタンパク尿を呈し，続いて低タンパク血症，高脂血症，腎性貧血が認められ，末期には腎不全に陥るという臨床像はすべての個体に共通の特性である。しかし全身性浮腫は雄個体に多くに認められるが，個体差が大きく，病態進行により軽減することもあり，注意を要する(図1)。病理組織学的には，生後間もなく形態学的に正常な糸球体基底膜(glomerular basement membrane：GBM)が完成した直後にGBMの肥厚および上皮細胞足突起の消失が認められ，この時点で糸球体の選択的透過性が破綻していることが分かっている[4]。続いてメサンギウム領域の拡張，糸球体基底膜へのIgG，IgM，IgAの沈着が認められ，急速に糸球体硬化が進行する。病態末期には尿細管の拡張，リンパ球の浸潤も認められ(図2)，最後は腎不全で死亡するがこの時期についても個体差が大きく，多くは5ヵ月齢以降に死亡する。

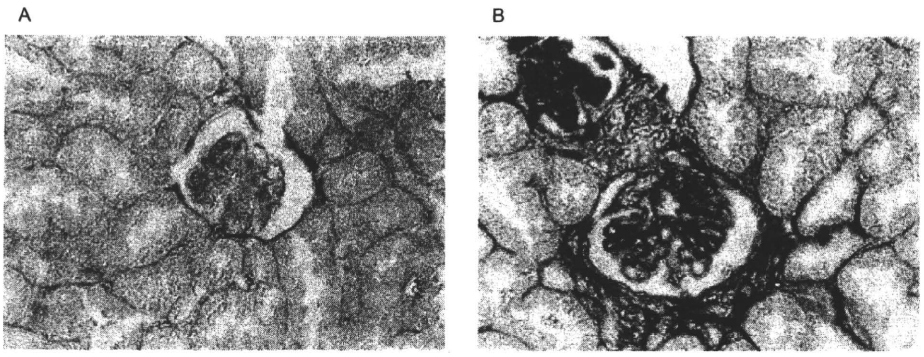

図2　発症初期(A)には認められない糸球体硬化，尿細管拡張，リンパ球浸潤が認められる病態末期の腎(B)

3. 腎線維症モデルとしての有用性

病態進行に伴って糸球体メサンギウム領域および尿細管間質にコラーゲン，ラミニン，フィブロネクチンなど細胞外マトリックス(ECM)の異常蓄積が認められることから，腎線維症モデルとして有用である[5](図3)。下述のように，ECM蓄積には産生亢進，分解抑制およびECM成分の修飾が原因となる。

＜産生亢進＞

ICGNマウスの腎においては，I型コラーゲンやIII型コラーゲンなどの間質性成分の顕著な産生亢進が認められることが特徴である。一方，基底膜成分であるIV型コラーゲン，ラミニンなども糸球体に顕著に蓄積しているものの産生亢進は軽度である。

＜分解抑制＞

ECMの分解を担うmatrix metalloproteinase(MMP)は，コラゲナーゼ(MMP-1など)，ゼラチナーゼ(MMP-2，MMP-9)，ストロメライシン(MMP-3など)，膜型MMP(MMP-14など)などに大別される。ICGNマウス腎においては，MMP-1，MMP-2，MMP-9の活性低下が認められたが，MMP-3は正常腎での活性と同程度であった[6]。特にMMP-2，MMP-9といった基底膜成分の分解に関与する酵素活性が低下していることからIV型コラーゲンなどの蓄積には分解系の抑制が深く関与していることが示唆された。

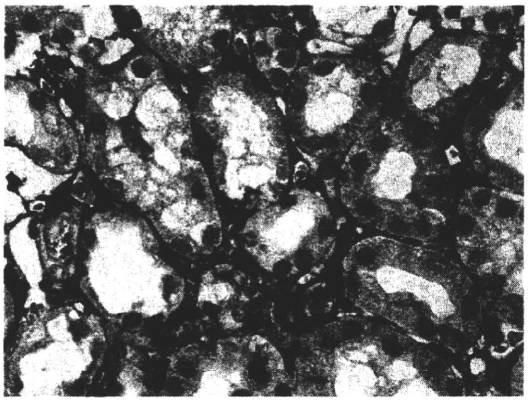

図3　尿細管間質部に細胞外マトリックス異常蓄積が認められる病態末期の腎

＜ECM成分修飾＞

Lysyl oxidase(LOX)はコラーゲンやエラスチンなどを修飾する酵素として知られる。ICGNマウス腎においてLOXが増加しており，ECM成分が修飾されていることが示唆されている[7]。修飾されたECM成分が分解を受けにくくなっていることも線維化進行に関与している可能性が高い。

これらのすべての現象について，その制御に深く関与する因子がtransforming growth factor(TGF)-β_1であり，腎だけではなく多くの臓器の線維化進行に関与している。その機能はECM産生を亢進するだけではなく，ECM分解酵素のインヒビターやLOXのような修飾酵素の発現をも亢進することなどの多面的な作用が知られており，線維化現象のkey moleculeである。ICGNマウスの腎においてもTGF-β_1が増加しており，線維化に寄与している。興味深いことに，このマウスではTGF-β_1の細胞内シグナル伝達因子であるsmad4が細胞内に増加することで尿細管間質病変を増悪させていることが分かっている[8]。もちろんTGF-β independentな線維化の機序についてもさらなる精査が必要である。このようにICGNマウス腎においてECM産生・分解・修飾の異常が認められることから，線維化メカニズムの解析や治療法の開発などに利用可能である。これまでにICGNマウスを腎線維症モデルとして利用してhepatocyte growth factor[9]やangiotensin-converting enzyme inhibitor[10]による腎線維症抑制効果が報告されている。

4. 腎性貧血モデルとしての利用

赤血球の産生を促進するホルモンとして知られるエリスロポエチン(erythropoietin：EPO)は，主に腎の尿細管間質細胞で産生されるので腎疾患が進行すると産生量が低下し，貧血が起こる。ICGNマウスでは尿細管間質病変の進行とともに貧血が認められるので腎性貧血モデルとして適している[11]。ヒト組換EPO投与(5 U/mouse/day 5日間反復)により，ヘモグロビン濃度とヘマトクリット値が正常になる[12]。

以上紹介してきたようにICGNマウスは，我が国発の数少ないネフローゼ症候群の特性を備えた遺伝性のモデル動物であるが，病状の個体差が大きいことや繁殖が難しいことが原因となって利用例は多くない。現在は(独)医薬基盤研究所実験動物研究資源バンク(http://animal.nibio.go.jp/)からマウスや凍結胚が購入可能である。できるだけ多くの方が活用してくださることを期待している。

参考文献

1) Ogura A., Asano T., Matsuda J., Noguchi Y., Yamamoto Y., Takano K. and Nakagawa M. : Development of nephrotic ICGN mice : the origin, reproductive ability, and incidence of glomerulonephritis. Exp. Anim., 38 : 349-352, 1989.

2) Ogura A., Asano T., Matsuda J., Takano K., Nakagawa M. and Fukui M. : Characteristics of mutant mice (ICGN) with spontaneous renal lesion: A new model for human nephrotic syndrome. Lab. Anim., 23 : 169-174, 1989.

3) Cho A.-R., Uchio-Yamada K., Torigai T., Miyamoto T., Miyoshi I., Matsuda J., Kurosawa T., Kon Y., Asano A., Sasaki N. and Agui T. : Deficiency of the tensin2 gene in the ICGN mouse, an animal model for congenital nephrotic syndrome. Mamm. Genome, 17 : 407-416, 2006.

4) Ogura A., Fujimura H., Asano T., Koura M., Naito I. and Kobayashi Y. : Early ultrastructural glomerular alteration in neonatal nephrotic mice (ICGN strain). Vet. Pathol., 32 : 321-323, 1995.

5) Uchio K., Manabe N., Kinoshita A., Tamura K., Miyamoto M., Ogura A., Yamamoto Y. and Miyamoto H. : Abnormalities of extracellular matrices and transforming growth factor β_1 localization in the kidney of the hereditary nephrotic mice (ICGN strain). J. Vet. Med. Sci., 61 : 769-776, 1999.

6) Uchio K., Manabe N., Tamura K., Miyamoto M., Yamaguchi M., Ogura A., Yamamoto Y. and Miyamoto H. : Decreased matrix metalloproteinase activity in the kidneys of hereditary nephrotic mice (ICGN strain). Nephron, 86 : 145-151, 2000.

7) Goto Y., Uchio-Yamada K., Anan S., Yamamoto Y., Ogura A. and Manabe N. : Transforming growth factor-β_1 mediated up-regulation of lysyl oxidase in the kidneys of hereditary nephrotic mouse with

chronic renal fibrosis. Virchows Arch., 47 : 1-10, 2005.

8) Goto Y., Manabe N., Uchio-Yamada K., Yamaguchi-Yamada M., Inoue N., Yamamoto Y., Ogura A., Nagano N. and Miyamoto H. : Augmented cytoplasmic Smad4 induces acceleration of TGF-β_1 signaling in renal tubulointerstitial cells of hereditary nephrotic ICGN mice with chronic renal fibrosis ; possible role for myofibroblastic differentiation. Cell Tissue Res., 315 : 209-221, 2004.

9) Mizuno S., Kurosawa T., Matsumoto K., Mizuno-Horikawa Y., Okamoto M. and Nakamura T. : Hepatocyte growth factor prevents renal fibrosis and dysfunction in a mouse model of chronic renal disease. J. Clin. Invest., 101 : 1827-1834, 1998.

10) Mizuno S., Horikawa Y., Okamoto M. and Kurosawa T. : Preventive effect of ACE inhibitor on interstitial myofibroblast formation and matrix deposition in a nephrotic model. Renal Failure, 20 : 481-491, 1998.

11) Yamaguchi-Yamada M., Manabe N., Uchio-Yamada K., Akashi N., Goto Y., Miyamoto Y., Nagao M., Yamamoto Y., Ogura A. and Miyamoto H. : Anemia with chronic renal disorder and disrupted metabolism of erythropoietin in ICR-derived glomerulonephritis (ICGN) mice. J. Vet. Med. Sci., 66 : 423-431, 2004.

12) Miyamoto Y., Kuramitsu-Miyamoto K., Iwanaga E., Uchio-Yamada K., Yamaguchi-Yamada M., Ogura A. and Manabe N. : Effect of human erythropoietin (hEPO) treatment on anemia in ICR-derived glomerulonephritis (ICGN) mice. Exp. Anim., 54 : 181-184, 2005.

（山田-内尾こずえ／眞鍋 昇）

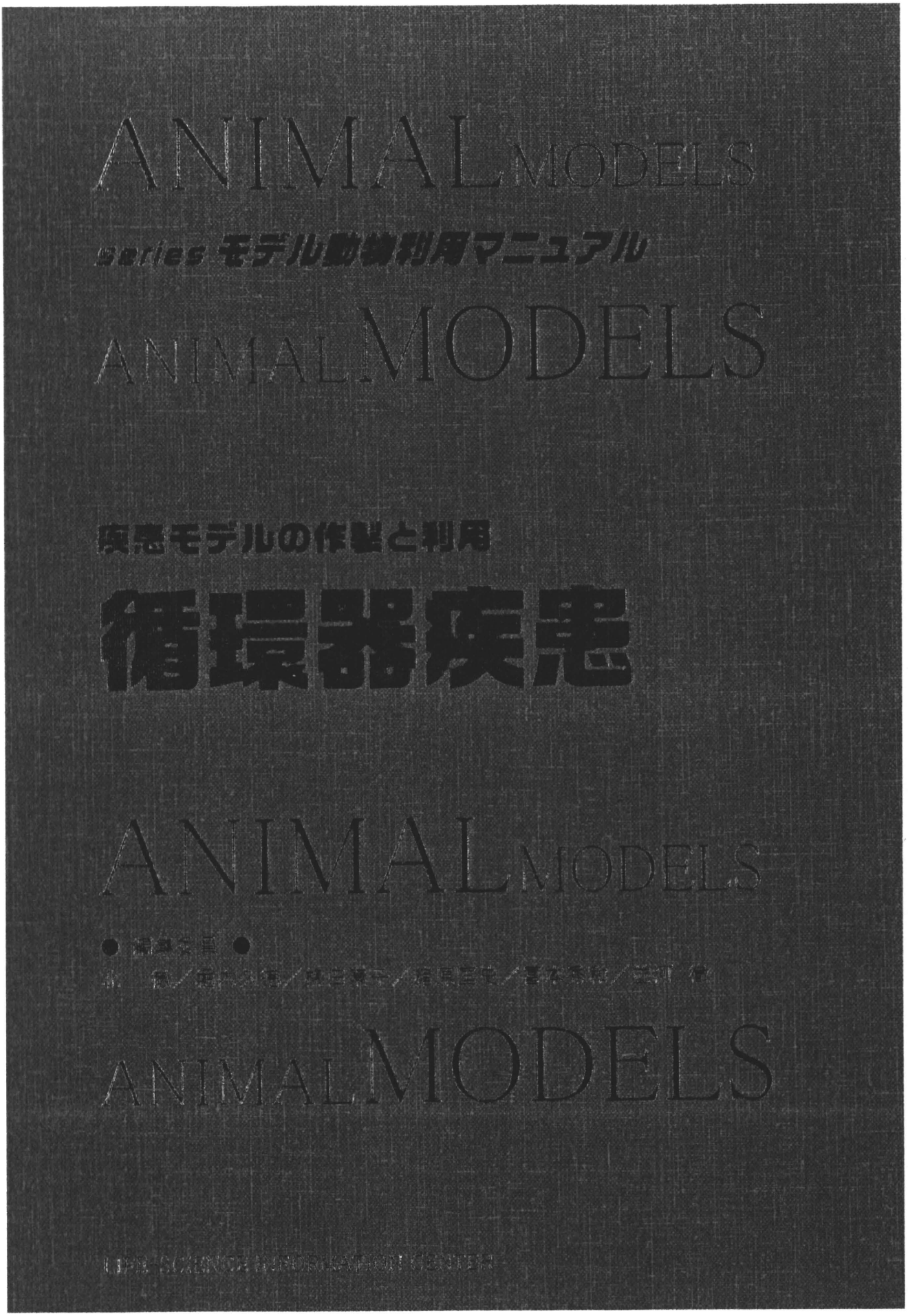
ANIMAL MODELS
Series モデル動物利用マニュアル
ANIMAL MODELS
疾患モデルの作製と利用
循環器疾患
ANIMAL MODELS
ANIMAL MODELS

J. Biochem. 2011;149(2):161–170 doi:10.1093/jb/mvq125

Increased globotriaosylceramide levels in a transgenic mouse expressing human α1,4-galactosyltransferase and a mouse model for treating Fabry disease

Received September 1, 2010; accepted October 14, 2010; published online October 19, 2010

Chikara Shiozuka[1], Atsumi Taguchi[1,2], Junichiro Matsuda[3], Yoko Noguchi[3], Takanori Kunieda[3], Kozue Uchio-Yamada[3], Hidekatsu Yoshioka[2], Ryoji Hamanaka[4], Shinji Yano[5], Shigeo Yokoyama[5], Kazuaki Mannen[6], Ashok B. Kulkarni[7], Koichi Furukawa[8] and Satoshi Ishii[1,2,9,*]

[1]Department of Agricultural and Life Sciences, Obihiro University of Agriculture and Veterinary Medicine, Obihiro, Hokkaido 080-8555; [2]Department of Matrix Medicine, Faculty of Medicine, Oita University, Yufu, Oita 879-5593; [3]Laboratory of Animal Models for Human Diseases, National Institute of Biomedical Innovation, Ibaraki, Osaka 567-0085; [4]Department of Cell Biology, Faculty of Medicine, Oita University, Yufu, Oita 879-5593; [5]Department of Diagnostic Pathology, Faculty of Medicine, Oita University, Yufu, Oita 879-5593; [6]Division of Laboratory Animal Sciences, Research Promotion Project, Oita University, Yufu, Oita 879-5593, Japan; [7]National Institute of Dental and Craniofacial Research, Bethesda, MD 20892, USA; [8]Department of Biochemistry II, Nagoya University School of Medicine, Nagoya, Aichi 466-0065; and [9]Biochemical Laboratory, GlycoPharma Corporation, Oita 870-0822, Japan

*Satoshi Ishii, Ph.D., Department of Matrix Medicine, Faculty of Medicine, Oita University, Hasama-cho Idaigaoka 1-1, Yufu-shi, Oita 879-5593, Japan, Tel: +81 97 586 5661, Fax: +81 97 546 2534, email: ishiis01@oita-u.ac.jp

Fabry disease is a lysosomal storage disorder caused by an α-galactosidase A (α-Gal A) deficiency and resulting in the accumulation of glycosphingolipids, predominantly globotriaosylceramide (Gb3). A transgenic mouse expressing the human α-Gal A R301Q mutant in an α-Gal A-knockout background (TgM/KO) should be useful for studying active-site-specific chaperone (ASSC) therapy for Fabry disease. However, the Gb3 content in the heart tissue of this mouse was too low to detect an ASSC-induced effect. To increase the Gb3 levels in mouse organs, we created transgenic mice (TgG3S) expressing human α1,4-galactosyltransferase (Gb3 synthase). High levels of Gb3 were observed in all major organs of the TgG3S mouse. A TgG3S (+/−)M(+/−)/KO mouse was prepared by cross-breeding the TgG3S and TgM/KO mice and the Gb3 content in the heart of the TgG3S(+/−)M(+/−)/KO mouse was 1.4 μg/mg protein, higher than in the TgM(+/−)/KO (<0.1 μg/mg protein). Treatment with an ASSC, 1-deoxygalactonojirimycin, caused a marked induction of α-Gal A activity and a concomitant reduction of the Gb3 content in the TgG3S(+/−) M(+/−)/KO mouse organs. These data indicated that the TgG3S(+/−) M(+/−)/KO mouse was suitable for studying ASSC therapy for Fabry disease, and that the TgG3S mouse would be useful for studying the effect of high Gb3 levels in mouse organs.

Keywords: active-site-specific chaperone therapy/Fabry disease/globotriaosylceramide/mouse model.

Abbreviations: A4GalT, α1,4-galactosyltransferase; ASSC, active-site-specific chaperone; α-Gal A, α-galactosidase A; DGJ, 1-deoxygalactonojirimycin; Gb3, globotriaosylceramide (Galα1,4Galβ1, 4Glc-Ceramide); GLAko mouse, α-Gal A knockout mouse; Gb4, globotetraosylceramide; G3Stg/GLAko mouse, transgenic mouse expressing human Gb3 synthase in α-Gal A knockout background; G3S/COS-7 cells, COS-7 cells expressing human Gb3 synthase; HPTLC, high-performance thin-layer chromatography; LacCer, lactosylceramide; PBS, phosphate-buffered saline; Stx1B, Shiga toxin 1 B-subunit; TgM/KO mouse, transgenic mouse expressing human mutant R301Qα-Gal A in α-Gal A knockout background; TgG3S mouse, transgenic mouse expressing human Gb3 synthase; TgG3S (+/−)M(+/−)/KO mouse, transgenic mouse expressing human Gb3 synthase and mutant R301Qα-Gal A in α-Gal A knockout background.

Fabry disease is an X-linked recessive disease caused by insufficient activity of lysosomal α-galactosidase A (α-Gal A, EC 3.2.1.22), an enzyme responsible for the catabolism of glycosphingolipids, predominantly globotriaosylceramide (Gb3) (*1*). Patients with Fabry disease show diverse clinical manifestations caused by generalized vasculopathy—pain in the extremities, hypohidrosis, angiokeratoma, corneal opacity, ischaemic heart disease, progressive nephropathy and cerebrovascular disease (*2*). Approximately 60% of the mutations reported in patients with Fabry disease are missense mutations in the α-Gal A gene. Although many products encoded by these missense mutations have normal catalytic properties, they also have low thermostability and degrade rapidly after their synthesis in the endoplasmic reticulum (ER) (*3–5*). A novel therapeutic strategy for the treatment of Fabry disease, which uses competitive inhibitors of α-Gal A as active-site-specific chaperones (ASSCs), has been suggested (*6–8*). The normal folding of those missense mutant enzymes can be restored by ASSC treatment, thus preventing excessive ER-associated degradation and improving the transport of the mutant enzyme to the lysosomes (*4*). Cultivation of patients' cells with an ASSC of α-Gal A [*e.g.* 1-deoxygalactonojirimycin (DGJ)] at low concentrations resulted in a substantial

increase in both residual enzyme activity and the amount of intracellular enzyme protein (*4*, *6*, *9*).

A mouse line deficient in α-Gal A (GLAko mice) was established in 1997 by disruption of the murine α-Gal A gene (*10*). Despite the accumulation of Gb3 in Fabry disease-relevant organs of the GLAko mice, the mice were clinically normal and had a typical life span. These mice have served as an excellent model for studies on enzyme replacement therapy (*11*), gene therapy (*12–14*) and substrate reduction therapy (*15*), wherein the increased α-Gal A activity and reduced Gb3 accumulation were primary objectives. However, this mouse model is not suitable for studying ASSC therapy, which requires the expression of a human mutant enzyme. In a previous report (*16*), we established a homozygous transgenic mouse in a murine α-Gal A knockout background (TgM/KO mouse) by crossbreeding a TgM mouse expressing the human α-Gal A R301Q mutant (*17*) in GLAko mice. Like the GLAko mouse, the TgM/KO mouse does not exhibit a disease phenotype, however these mice do express human mutant α-Gal A and serve as an excellent biochemical model for studying ASSC (*18*). Heterozygous TgM/KO mice show a lower α-Gal A activity than the homozygotes, and Gb3 accumulates in the kidney of the heterozygous mouse, but not in the heart, which is affected in Fabry disease (*16*).

The purpose of this study was to establish a transgenic mouse that expressed high levels of Gb3 as well as the human mutant α-Gal A enzyme in heart tissue, which would permit us to assess the effect of ASSC (enhancement of α-Gal A activity and decrease in Gb3 accumulation) in the heart. Here, in order to increase cardiac Gb3 production, we simply overexpressed human α1,4-galactosyltransferase [*A4GalT*, Gb3 synthase (G3S, EC 2.4.1.228)] to obtain the TgG3S mouse line. We confirmed that these mice expressed high levels of Gb3 in their major organs, and then bred them with the TgM/KO mice to obtain TgG3S(+/−)M(+/−)/KO mice. Here we report the characterization and potential usefulness of this new mouse line.

Materials and Methods

Establishment of a stable transformant expressing A4GalT in COS-7 cells and A4GalT-overexpressing transgenic mice (TgG3S)

The human Gb3 synthase (G3S) cDNA containing the full-length coding sequence and an *Eco*RI site at both ends was prepared by polymerase chain reaction (PCR) using a Phusion™ High-Fidelity PCR Kit [New England BioLabs (NEB), Ipswich, MA, USA]. The cDNA for α1,4Gal-TpVTR1 (*19*) was the template, and the primer sequences were 5′-TGGGAATTCCATGTCCAAGCC-3′ and 5′-GGGGAATTCACAAGTACATTTTCATGGC-3′. The 1.1-kb PCR product was purified with a PCR Purification Kit (QIAGEN K.K., Japan) and digested with *Eco*RI (NEB). The digested cDNA was subcloned into the *Eco*RI site of expression vector pCXN2 (*20*), and the product was designated as pCXN2-G3S. For the preparation of the stably transformed G3S/COS-7 cells, pCXN2-G3S was linearized with *Hind*III (NEB) and then transfected into COS-7 cells with the FuGENE™6 transfection reagent (Roche Molecular Biochemicals, Basel, Switzerland), according to the manufacturer's protocol. Stably transformed G3S/COS-7 cells were selected by growing them in culture medium containing 400 μg/ml of G418 (Sigma, St Louis, MO, USA) for 4 weeks.

A DNA fragment comprising a mammalian expression unit and the human Gb3 synthase cDNA was prepared by digesting the pCXN2-G3S with *Sal*I and *Bam*HI (NEB). A fragment that was ~3.5 kb was isolated by agarose gel electrophoresis and purified by a Gel Extraction Kit (QIAGEN). A transgenic mouse (TgG3S) expressing human Gb3 synthase was generated by injecting the DNA fragments into the pronuclei of fertilized eggs taken from superovulated C57BL/6J Jms female mice, and the embryos were implanted into pseudopregnant Jcl:MCH mice, as described previously (*21*). Transgenic founder mice were identified by PCR with a primer set (5′-ATTGTTCTCAAGAACCTGCG-3′ and 5′-ATTTGTGAGCC AGGGCATTG-3′). A transgene fragment was confirmed as a single 548-bp band on agarose gel electrophoresis. To generate an animal model exclusively expressing both human G3S and human mutant α-Gal A in an endogenous *GLA* knockout background [TgG3S(+/−)M(+/−)/KO mice], we first prepared a mouse line overexpressing the human G3S transgene in an α-Gal A knockout background (G3Stg/GLAko) by crossbreeding male TgG3S mice and homozygous female GLAko mice (since *GLA* is located on the X chromosome). After the G3Stg/GLAko mouse line was established, TgM/KO and G3Stg/GLAko mice were crossbred to obtain TgG3S(+/−)M(+/−)/KO mice.

Determination of A4GalT mRNA expression in mouse tissues

The *A4GalT* mRNA expression of the transgene (human *A4GalT*) was determined by a reverse transcriptase (RT)-PCR using Takara RNA PCR Kit (AMV) Ver.3.0 (Takara Bio Inc., Shiga, Japan). The total RNA samples from tissues of wild-type and transgenic mice were prepared with RNAiso (Takara Bio Inc.), and the RNA concentrations were determined by absorbance at 260 nm. The RT reaction was performed at 30°C for 10 min, and then at 42°C for 15 min, followed by incubation at 99°C for 5 min. PCR amplification was performed using the following conditions: initial denaturation (94°C, 5 min) followed by 30 cycles of denaturation at 94°C for 30 s, annealing at 58°C for 30 s, elongation at 72°C for 30 s and further elongation at 72°C for 2 min. The DNA fragment (409 bp), which contained a sequence that is highly conserved between the mouse and human *A4GalT* genes, was amplified with primers 5′-GGCATC TC(A/T)CTTCTGAGCTG-3′ and 5′-GGATGGAACACCACTTC TTG-3′. PCR products were run on a 2% agarose gel, stained with ethidium bromide and photographed. The glyceraldehyde-3-phosphate dehydrogenase (GAPDH) gene was used as an expression control gene as described previously (*22*).

Administration of DGJ to TgG3S(+/−)M(+/−)/KO mice

TgG3S(+/−)M(+/−)/KO mice were supplied with fresh tap water *ad libitum* and rodent pellets. DGJ (Toronto Research Chemicals, Toronto, Canada) was administrated to one group of female TgG3S(+/−)M(+/−)/KO mice in tap water as a DGJ aqueous solution without any other substances. After 4 weeks, the animals were sacrificed and the organs were quickly removed and rinsed with phosphate-buffered saline (PBS). Tissue homogenates were subjected to enzyme assays and lipid extraction.

Assay of enzyme activity and protein content

All samples were kept on ice and processed as rapidly as possible. Approximately 10% (w/v) tissue homogenates were prepared in water using a micro-homogenizer (Physcotron, Niti-on Inc., Chiba, Japan). The supernatant obtained from the homogenate after centrifugation at 10,000*g* for 5 min was used in the enzyme assays. The α-Gal A activity was assayed with 4-methylumbelliferyl α-D-galactoside (Sigma) as the substrate and N-acetyl-D-galactosamine (75 mM) as the inhibitor for α-N-acetylgalactosaminidase in 0.1 M sodium citrate buffer (pH 4.6) as described previously (*16*). The protein concentration was determined using a DC Protein Assay kit (Bio-Rad Laboratories, Hercules, CA, USA) with bovine serum albumin as the standard.

Detection of neutral and acidic glycosphingolipids by thin-layer chromatography analysis

Glycosphingolipids were extracted from cultured cells and mouse tissues and were analysed as described previously (*14*), with some modifications. Crude lipids were extracted from cultured cells (eq. to 1 mg of protein) and tissue homogenates (eq. to 5 mg of protein), using a mixture of chloroform:methanol (2:1, v/v). Glycosphingolipids were dried under a stream of nitrogen.

The dried samples were dissolved in chloroform : methanol : water (30 : 60 : 8, v/v) and applied to a TOYOPEARL DEAE-650 column (Tosoh Corporation, Tokyo, Japan). The column was washed with chloroform : methanol : water (30 : 60 : 8, v/v). The pass-through fraction was pooled for the preparation of neutral glycosphingolipids. The acidic glycosphingolipids including gangliosides were eluted with chloroform : methanol : 0.8 M sodium acetate (30 : 60 : 8, v/v), and they were desalted with Sep-Pak C18 reverse-phase cartridge (Waters, Milford, MA, USA) and then analysed by thin-layer chromatography (TLC). The neutral glycosphingolipids fraction was dried, and then subjected to mild alkaline treatment with 1 ml of 0.1 N NaOH in methanol at 40°C for 2 h. After neutralizing the solution with glacial acetic acid, glycosphingolipids were further subjected to the Folch's partition (choloroform : methanol : H_2O, 8 : 4 : 3 in v/v/v), recovered in the lower phase, and then quantitatively applied to TLC plates. TLC analyses were performed with HPTLC-Silica gel 60 plates (Merck & Co., Inc., Whitehouse Station, NJ, USA) using a solvent system of chloroform : methanol : water (60 : 35 : 8, v/v/v) and chloroform : methanol : 0.2% $CaCl_2$ (60 : 35 : 8, v/v/v) for the separation of neutral and acidic glycosphingolipids, respectively. Glycosphingolipids were detected by spraying the plate with orcinol-sulphuric acid reagent, and heating the plate at 110°C. The Gb3 from porcine erythrocytes was purchased from Nakalai Tesque (Kyoto, Japan), and other glycosphingolipid standards were purchased from Wako Pure Chemicals (Osaka, Japan). The ganglioside standards from bovine brain (GM1, GM2 and GM3) were purchased from Wako.

Binding assay

The Stx1B binding assay was performed as described previously (*23*), with some modifications. After glycosphingolipids were separated by TLC as described above, a TLC plate was sunk in a 0.4% polyisobutylmethacrylate (GlycoTech, Rockville, MD, USA) solution (2.5% polyisobutylmethacrylate in chloroform was diluted to 0.4% with hexane) and then blocked with 1% bovine serum albumin in PBS (BSA-PBS). The plate was incubated with 2.5 μg/ml of Stx1B in BSA-PBS at room temperature for 20 min and washed with PBS. After incubation with 7.0 μg/ml of anti-Stx1B polyclonal antibody (produced in rabbits with purified Stx1B) for 20 min the plate was washed with PBS. After further incubation with horseradish peroxidase-conjugated anti-rabbit IgG (Pierce Chemical, Rockford, IL, USA) at room temperature for 20 min and the following final washing, Stx1B-binding was visualized with an enhanced chemiluminescent substrate (Pierce).

Immunoelectron microscopy

The G3S/COS-7 cells were cultured with or without 10 mM DGJ for 4 days, then fixed in 2% glutaraldehyde in 0.2 M phosphate buffer (pH 7.4) for 3 h; they were then further incubated in 1% osmium tetraoxide for 2 h, dehydrated in ethanol and embedded in Epok 812. Immunoelectron microscopy was performed as described previously (*24*). In summary, each thin section was briefly microwaved in Target Retrieval Solution, pH 10 (DAKO, Carpinteria, CA, USA) and then incubated for 30 min at room temperature with Stx1B (2.5 μg/ml). After being washed with Wash Buffer [50 mM Tris–HCl (pH 7.6) containing 0.8% NaCl and 0.1% BSA], the ultrathin section was incubated with anti-Stx1B antibody (7 μg/ml). After another wash, the section was incubated with gold-conjugated goat anti-rabbit IgG. The section was then washed again, stained with uranyl acetate and lead citrate, and examined using a transmission electron microscope (JEM-1200EXII, JEOL, Akishima, Tokyo, Japan).

Results

Establishment of TgG3S mice

First, we prepared a stable transformant COS-7 cell line expressing Gb3 synthase (G3S/COS-7 cells) to confirm that the expression construct prepared in our present study could increase intracellular Gb3 content. We extracted neutral glycosphingolipids from the cells and quantitated them by high performance TLC (HPTLC) (Fig. 1). The Gb3 and globotetraosylceramide (Gb4) levels in the G3S/COS-7 cells were markedly higher than those in the parental COS-7 cells or in a control line transformed with only the empty vector. The content of lactosylceramide (LacCer) in the G3S/COS-7 cells was lower than it was in the COS-7 cells, indicating that the expression product from the *A4GalT* gene in our construct catalysed the construction of Gb3 from LacCer.

A mouse line expressing the *A4GalT* gene (TgG3S) was generated by injecting the DNA fragment into the pronuclei of fertilized mouse ova taken from C57BL/6J female mice. A marked increase in the expression of the *A4GalT* gene in heart, kidney, liver, spleen, small intestine, brain, lungs and muscle of the TgG3S mice compared with wild-type C57BL/6J mice was observed by RT-PCR (Fig. 2A). High levels of Gb3 synthase expression resulted in an increase in Gb3 levels of all organs examined in this study (Fig. 2B). A glycosphingolipid band (possibly galabiosylceramide) with an Rf value similar to that of LacCer by HPTLC was also increased in the kidney and brain of the TgG3S mouse. No change was observed in the content of acidic glycosphingolipids including gangliosides in organs of TgG3S mice (data not shown). The TgG3S mouse line did not show any clinical phenotype and had a typical life span.

Preparation of TgG3S(+/−)M(+/−)/KO mouse line as a model mouse for ASSC therapy

To study the effect of ASSC on Gb3 content in the heart, we tried to increase the cardiac Gb3 content of the TgM/KO mouse by introducing the G3S-overexpressing transgene. The TgG3S(+/−)M(+/−)/KO mouse was created by crossbreeding the G3Stg/GLAko mouse and the TgM/KO mouse. The Gb3 content in the TgG3S(+/−)M(+/−)/KO heart and kidney was determined and compared with that in

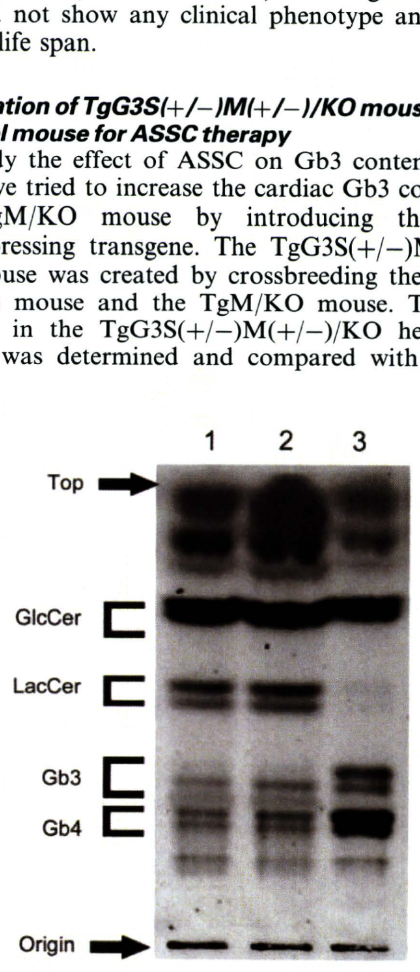

Fig. 1 Neutral glycosphingolipids in stably transformed G3S/COS-7 cells. Neutral glycosphingolipids were extracted from cell homogenates (containing 1 mg protein), as described in 'Materials and Methods' section. Glycosphingolipids were visualized with orcinol-sulphuric acid reagent. Lane 1, intact COS-7 cells; lane 2, mock transfection; lane 3, stable transformant G3S/COS-7 cells.

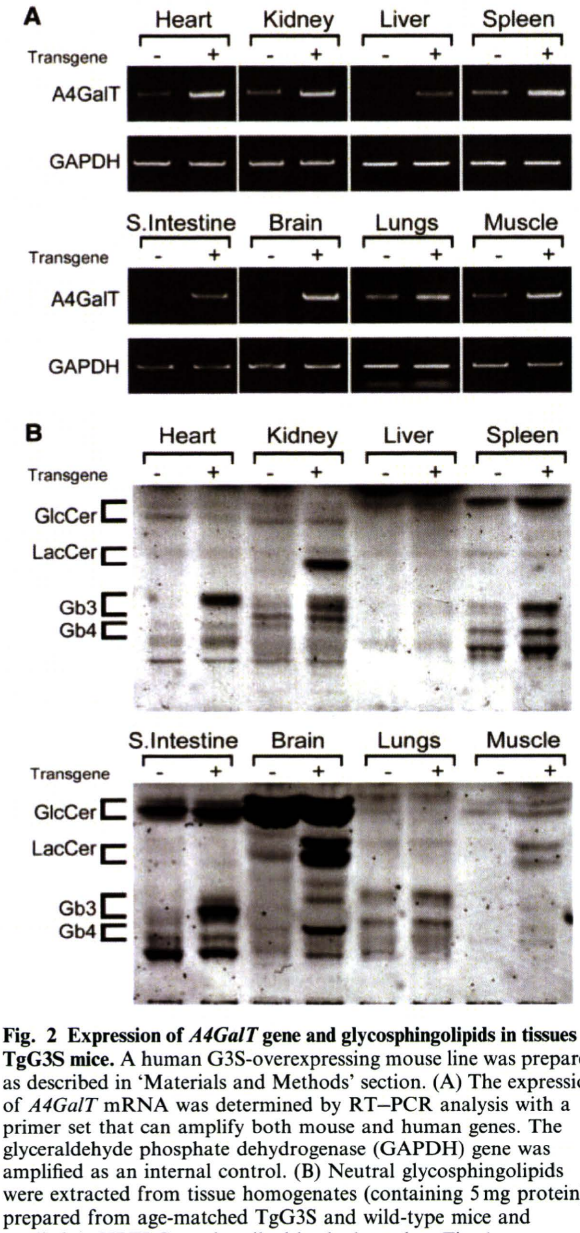

Fig. 2 Expression of *A4GalT* gene and glycosphingolipids in tissues of TgG3S mice. A human G3S-overexpressing mouse line was prepared as described in 'Materials and Methods' section. (A) The expression of *A4GalT* mRNA was determined by RT–PCR analysis with a primer set that can amplify both mouse and human genes. The glyceraldehyde phosphate dehydrogenase (GAPDH) gene was amplified as an internal control. (B) Neutral glycosphingolipids were extracted from tissue homogenates (containing 5 mg protein) prepared from age-matched TgG3S and wild-type mice and applied to HPTLC, as described in the legend to Fig. 1.

wild-type C57BL/6J, TgG3S(+/−) and TgM(+/−)/KO mice (Fig. 3). A Gb3 level as high as that of the TgG3S mice (1.3 ± 0.3 μg/mg protein) was observed in the heart of the TgG3S(+/−)M(+/−)/KO mice (1.1 ± 0.3 μg/mg protein) (Fig. 3A). Furthermore, when we probed the HPTLC plate with Shiga toxin 1 B-subunit (Stx1B), which selectively binds Gb3, we did not detect Gb3 in the heart tissue of mouse lines that did not express the *A4GalT* transgene (*i.e.* wild-type and TgM(+/−)/KO mice) (Fig. 3C). In contrast, Gb3 was detectable in kidney tissue of all the mouse lines, and a slight increase was observed in the lines expressing the *A4GalT* transgene (Fig. 3B, D and F). The *A4GalT* transgene did not change the α-Gal A activity in either the heart or kidney (Fig. 3G and H). Marked increase in Gb3 content was detected in the heart and kidney by the expression of Gb3 synthase, however no abnormality was observed in the histological examination of both organs from TgG3S(+/−)M(+/−)/KO mouse (data not shown).

Age-related increase in the kidney Gb3 content in TgG3S(+/−)M(+/−)/KO mice

The Gb3 content in the kidney of both the TgM(+/−)/KO and the TgG3S(+/−)M(+/−)/KO mice increased ~3-fold between 5 and 10 weeks of age (Fig. 4A and B). In contrast, neither the Gb3 content in the heart nor the α-Gal A activity in the heart or kidney changed during this time (Fig. 4B–D). These data showed that we needed to use age-matched TgG3S(+/−)M(+/−)/KO mice to determine the effect of DGJ on Gb3 content in the kidney. Because the change in the Gb3 content in the kidney changed relatively little between 10 and 15 weeks of age, we used mice in this age range to study the effects of DGJ treatment.

Effect of 0.05 mM DGJ treatment on Gb3 content in heart and kidney of TgG3S(+/−)M(+/−)/KO mice

DGJ was administrated to TgG3S(+/−)M(+/−)/KO mice in their water as a 0.05 mM solution, available *ad libitum*, for 4 weeks. Based on the daily water consumption, the DGJ dosage was calculated to be ~3 mg/kg body weight/day. In the heart tissues of TgG3S(+/−)M(+/−)/KO mice after treatment with DGJ, a 0.69-fold decrease in Gb3 content (1.44 ± 0.38 and 0.99 ± 0.40 μg/mg protein in control and DGJ-treated mice, respectively) was observed, along with a 5.4-fold increase in α-Gal A activity (24.7 ± 7.6 and 133.0 ± 24.9 unit/mg protein in control and DGJ-treated mice, respectively) (Fig. 5). Likewise, the Gb3 content of the kidney tissue decreased 0.61-fold (6.56 ± 1.33 and 3.97 ± 0.57 μg/mg protein in control and DGJ-treated mice, respectively), and the α-Gal A activity in the kidney increased 4.4-fold (6.4 ± 3.1 and 28.0 ± 2.8 unit/mg protein in control and DGJ-treated mice, respectively) after treatment. These data indicate that the enhancement of the mutant α-Gal A activity by treatment with DGJ reduced the Gb3 content of the heart as well as the kidney, and that the TgG3S(+/−)M(+/−)/KO mouse line is a useful mouse model for the study of ASSC treatment in Fabry disease-relevant organs.

Inhibitory effect of high-concentration DGJ on α-Gal A activity causes Gb3 accumulation in G3S/COS-7 cells

To determine the critical concentration of DGJ required to reduce the Gb3 accumulation of mammalian cells, G3S/COS-7 cells were cultured in DGJ (0–10 mM)-supplemented medium for 4 days. Significant Gb3 accumulation was observed in cases where DGJ dosage was >1 mM (Fig. 6A and B). As an explanation, we found that DGJ decreased the intracellular α-Gal A activity at these higher concentrations, although it slightly increased the α-Gal A activity at 10 μM DGJ, by the ASSC effect (Fig. 6C).

To confirm that the Gb3 accumulated in the lysosomes of the G3S/COS-7 cells, an immunoelectron microscopic study was conducted using the Stx1B and anti-Stx1B polyclonal antibodies to label the

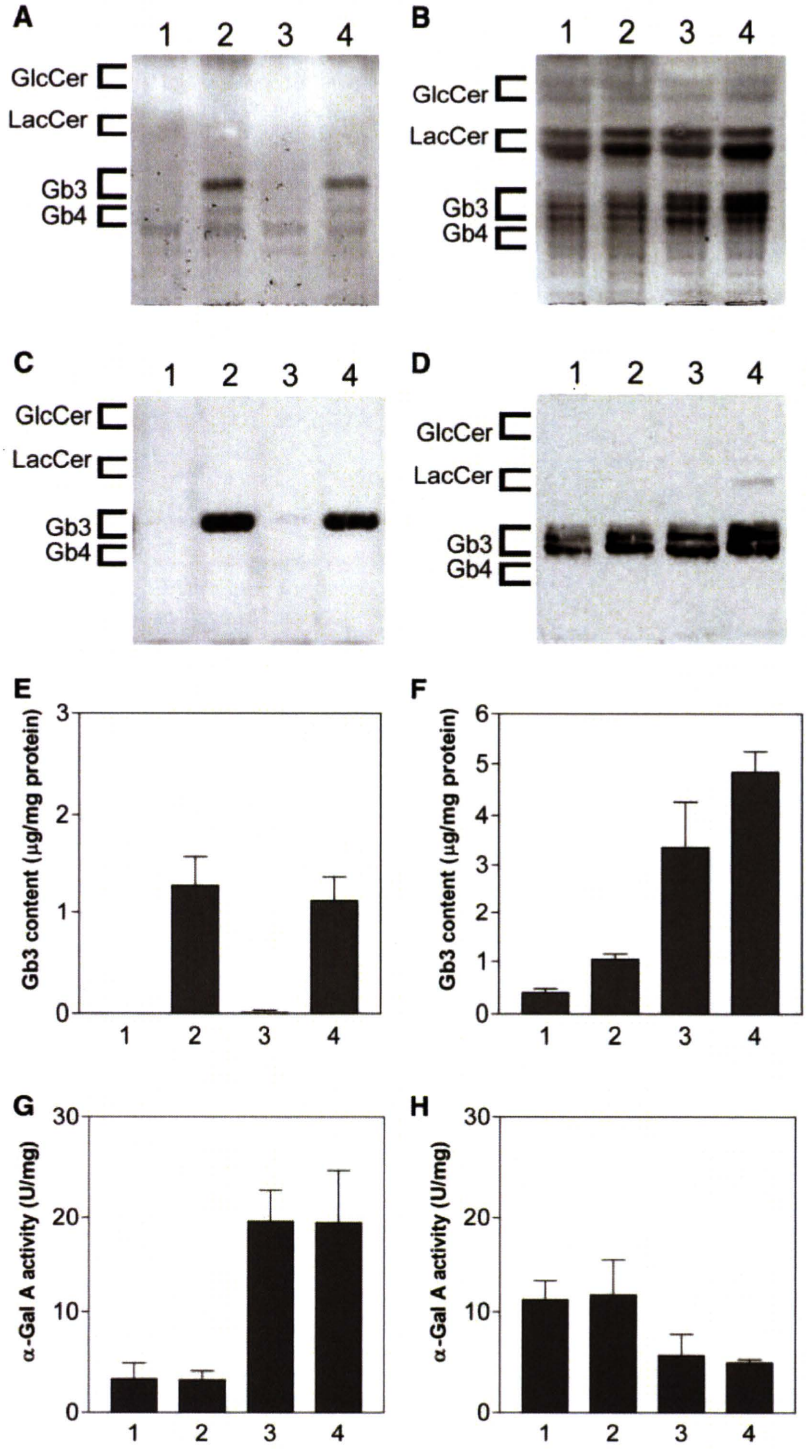

Fig. 3 Characterization of TgG3S(+/−)M(+/−)/KO mouse line. Gb3 content and α-Gal A activity in heart (A, C, E, and G) and kidney (B, D, F, and H) tissue from 10-week-old TgG3S(+/−)M(+/−)/KO mice were compared to those from age-matched mice from other lines. In (A–H), the lanes and columns show results from the following genotypes: 1, wild-type; 2, TgG3S(+/−); 3, TgM(+/−)/KO; 4, TgG3S(+/−)M(+/−)/KO. The neutral glycosphingolipids were extracted and visualized with orcinol-sulphuric acid reagent (A and B) or by Stx1B-binding (C and D). The Gb3 content (E and F) and α-Gal A activity (G and H) were determined as described in 'Materials and Methods' section.

Gb3 (Fig. 6D and E). The number of gold particles in each lysosome was markedly increased in the samples treated with 10-mM DGJ, indicating that the Gb3 had accumulated in them.

Administration of DGJ at high concentrations to TgG3S(+/−)M(+/−)/KO mice

To elucidate whether high concentrations of DGJ would also cause Gb3 accumulation in mouse tissues,

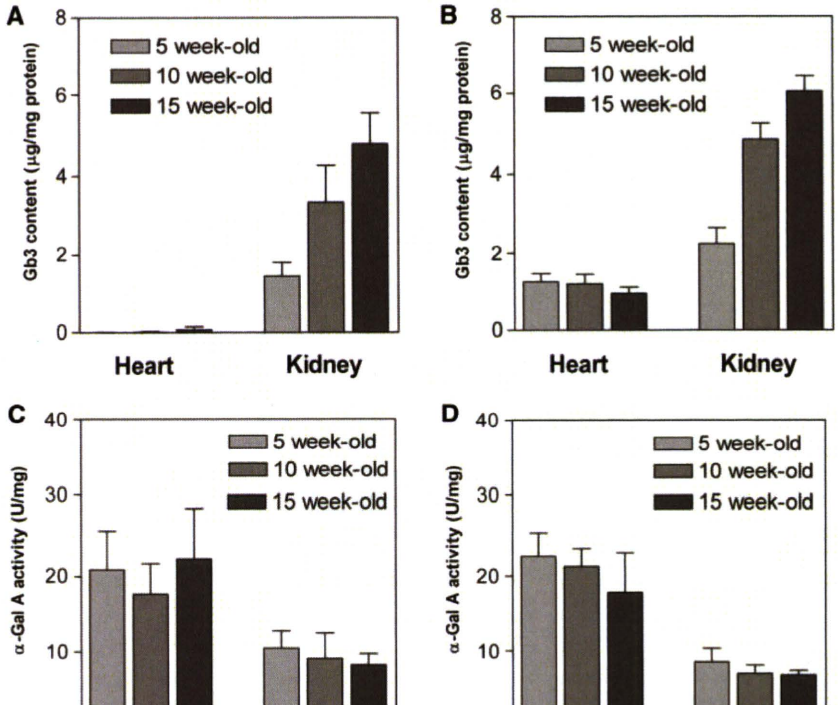

Fig. 4 Developmental changes in Gb3 content and α-Gal A activity in mouse heart and kidney. The Gb3 content and α-Gal A activity in the heart and kidney of TgM(+/−)/KO (A and C) and TgG3S(+/−)M(+/−)/KO mice (B and D) were determined at the indicated ages, as described in 'Materials and Methods' section. Each bar represents the means ± SD of data from three or four mice.

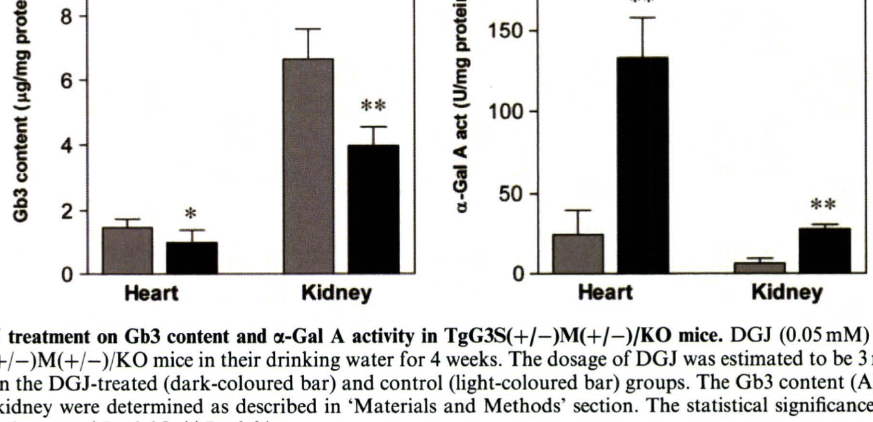

Fig. 5 Effect of DGJ treatment on Gb3 content and α-Gal A activity in TgG3S(+/−)M(+/−)/KO mice. DGJ (0.05 mM) was administrated to 10-week-old TgG3S(+/−)M(+/−)/KO mice in their drinking water for 4 weeks. The dosage of DGJ was estimated to be 3 mg/kg/day. Six female mice each were used in the DGJ-treated (dark-coloured bar) and control (light-coloured bar) groups. The Gb3 content (A) and α-Gal A activity (B) in the heart and kidney were determined as described in 'Materials and Methods' section. The statistical significance of the difference was determined by Student's *t* test. $*P<0.05$, $**P<0.01$.

TgG3S(+/−)M(+/−)/KO mice (three 10-week-old female mice for each group) were treated with DGJ at 5-fold (0.25 mM) and 25-fold (1.25 mM) higher concentrations than in the original experiment, for 4 weeks. No significant increase in Gb3 content either in heart or kidney tissue was observed after treatment with DGJ at high concentrations, and the low level of Gb3 in the TgG3S(+/−)M(+/−)/KO mouse tissues (~1.0 and 3.7 μg/mg protein in heart and kidney, respectively) was maintained (Fig. 7A and B), compared to that of age-matched G3Stg/GLAko mice (14 and 38 μg/mg protein in heart and kidney, respectively), which have no α-Gal A activity in their organs. Likewise, DGJ increased α-Gal A activity dose-dependently in the heart and kidney of the TgG3S(+/−)M(+/−)/KO mice (Fig. 7C and D). These data indicated that at least a 25-fold higher DGJ concentration (75 mg/kg body weight/day) may be safe for the treatment of patients with Fabry disease.

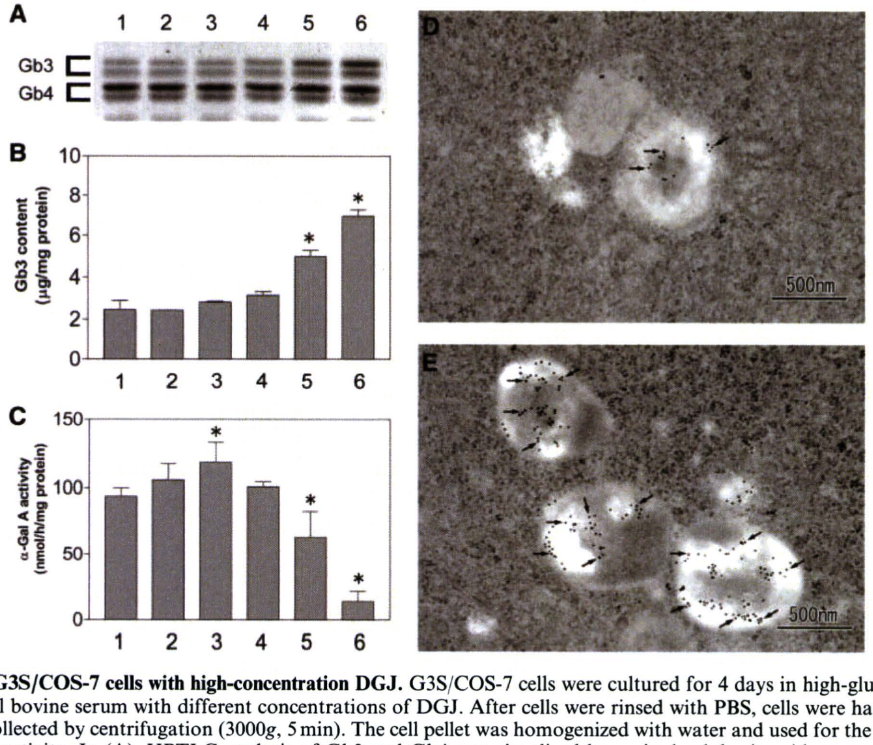

Fig. 6 Treatment of G3S/COS-7 cells with high-concentration DGJ. G3S/COS-7 cells were cultured for 4 days in high-glucose DMEM medium containing 10% foetal bovine serum with different concentrations of DGJ. After cells were rinsed with PBS, cells were harvested with PBS by a plastic scraper, and collected by centrifugation (3000*g*, 5 min). The cell pellet was homogenized with water and used for the determination of Gb3 content and α-Gal A activity. In (A), HPTLC analysis of Gb3 and Gb4 was visualized by orcinol-sulphuric acid reagent. The values of Gb3 content (B) and α-Gal A activity (C) are the means ± SD from three cultures. The statistical significance of the difference was determined by Student's *t* test; $*P<0.05$ versus DGJ-free culture. In (A, B and C), lanes and columns are the same, and 1, DGJ-free control culture; 2, 1 μM DGJ; 3, 10 μM DGJ; 4, 100 μM DGJ; 5, 1 mM DGJ; 6, 10 mM DGJ. The accumulation of Gb3 in lysosomes was determined by Stx1B-binding immunoelectron microscopic study in DGJ-free (D) and 10 mM DGJ-treated G3S/COS-7 cells (E). The ultrathin sections were incubated with Stx1B, then with anti-Stx1B polyclonal antibody, followed by immunogold labeling. Typical gold particles are pointed out by arrows.

Discussion

To increase the Gb3 content in mouse tissues, we tried overexpressing human Gb3 synthase in them. Since high Gb3 content was observed in tissues of the TgG3S mouse compared with wild-type mouse organs (Fig. 2), Gb3 synthase may be a critical enzyme for the synthesis of Gb3 in mouse organs, particularly in the heart and small intestine, where the increase was greatest. The increase in the tissue Gb3 level was determined by the binding of Stx1B (Fig. 3), which selectively binds Gb3 (*25*, *26*). The effect of G3S-overexpression on Gb3 content was greater in the heart than in the kidney, indicating that Gb3 synthase is expressed at low levels in wild-type mouse heart. The absence of Gb3 in the TgM/KO mouse heart was caused not only by its low expression of the Gb3 synthase gene, but also by the high activity of the mutant α-Gal A. However, the G3S-stimulated Gb3 production outstripped Gb3's decomposition by α-Gal A activity in the heart of the TgG3S (+/−)M(+/−)/KO mouse, leading to the accumulation of Gb3 (even though the Gb3 content was still lower than it was in the kidney).

We did not identify the neutral glycolipid, which has a similar Rf value to that of LacCer on HPTLC and which increased in the kidney and brain tissues in response to G3S-overexpression. However, it may be galabiosylceramide (Galα1,4Gal-Cer), since this glycolipid can be made by Gb3 synthase (*19*), and galactosylceramide (Gal-Cer) is produced in the kidney as well as in the brain (*27*).

The kidney Gb3 level increased with age in both TgM(+/−)/KO and TgG3S(+/−)M(+/−)/KO mice (Fig. 4). However, the α-Gal A activity was not changed in kidney tissue by the additional expression of the Gb3 synthase gene, and an increase in the kidney Gb3 level with age was also reported in GLAko mice (*28*), indicating that the age-related Gb3 accumulation in the kidney is not caused by a decrease in the catabolism of Gb3. Although the mechanism by which kidney Gb3 levels increase with age is unknown, these findings meant that we had to use age-matched mice to determine the ASSC effect on the kidney Gb3 level.

After successfully increasing the heart Gb3 level in mice, we were able to examine the ASSC effect of DGJ on Gb3 content in the heart tissue of TgG3S(+/−)M(+/−)/KO mice. A significant reduction of Gb3 in the heart was observed following treatment with 0.05 mM DGJ for 4 weeks, indicating that TgG3S(+/−)M(+/−)/KO mice are a useful animal model for determining the effect of ASSC therapy. A recent report on ASSC by Khanna *et al.* (*29*) using model mice also demonstrated that treatment with DGJ decreases the Gb3 level in the mouse heart. Although they used the same human mutant α-Gal A (R301Q) cDNA for the preparation of a model mouse, their strategy was very different from ours. Their mouse model, which shows Gb3 accumulation in heart

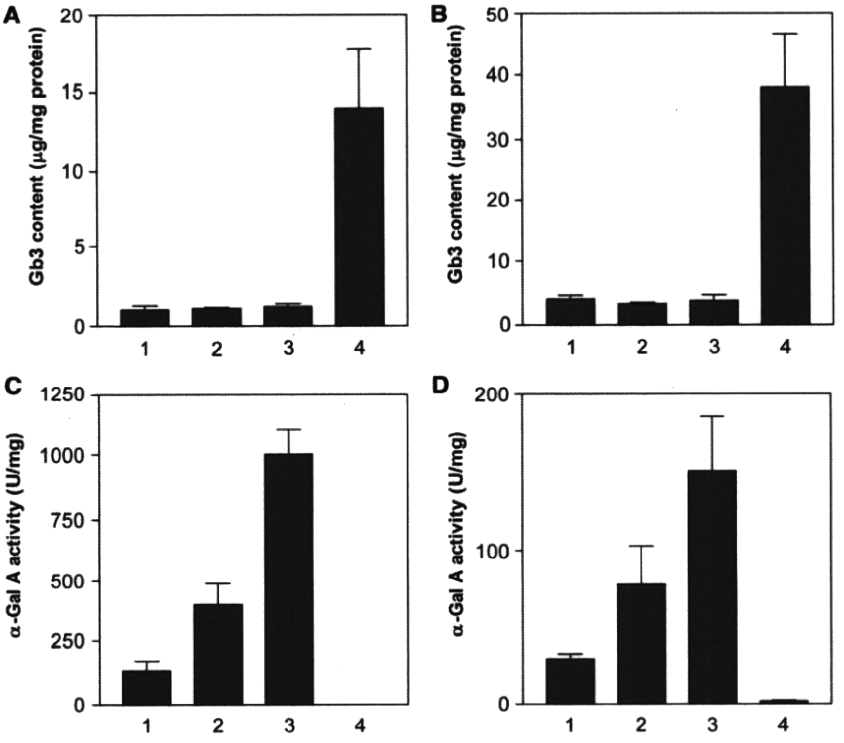

Fig. 7 Administration of high concentrations of DGJ to TgG3S(+/−)M(+/−)/KO mice. High concentrations of DGJ were administered to TgG3S(+/−)M(+/−)/KO mice (three or four 11-week-old female mice in each group) for 4 weeks. The Gb3 content and α-Gal A activity in the heart (A and C, respectively) and in the kidney (B and D, respectively) were determined as described in 'Materials and Methods' section. Lanes in A–D were the same, and lane 1, 0.05 mM DGJ treated; lane 2, 0.25 mM DGJ treated; and lane 3, 1.25 mM DGJ treated TgG3S(+/−)M(+/−)/KO mice, and lane 4, age-matched TgG3S(+/−)/KO mice.

tissues, was prepared by reducing the expression level of the mutant α-Gal A gene by using the human GLA promoter—which is a very weak promoter— instead of the stronger CAG (cytomegalovirus immediate-early enhancer/chicken β-actin hybrid) promoter. In contrast, we prepared a mouse model overexpressing both Gb3 synthase and the mutant α-Gal A genes. Our study confirmed the work of Khanna *et al.* (*29*) by reproducing their findings on the effect of DGJ in the heart, in a different mouse model. Although the effect of ASSC on Gb3 content can be determined in our mice and mice reported by Khanna *et al.* (*29*), the benefit of our mice is to be able to determine the localization and content of mutant enzyme in mice tissue with its antibody (*16*, *18*) as well as the localization of Gb3. Our mice will be useful for the elucidation of the mechanism of ASSC effect in detail by the detection of both mutant enzyme and Gb3 at the same time.

Although treatment with DGJ at a low concentration (<100 μM) can increase mutant α-Gal A activity, at high concentrations (>1 mM) DGJ significantly inhibits α-Gal A (*30*), leading to a corresponding increase in Gb3 levels in G3S/COS-7 cells (Fig. 6). Here, the increase in Gb3 content correlated with a decrease in the intracellular α-Gal A activity, and we used immunoelectron microscopy to show that Gb3 accumulated in the lysosomes of G3S/COS-7 cells treated with 10 mM DGJ. These data demonstrate the importance of determining a safe and effective concentration of DGJ for use in clinical therapy. In our present study, we used a 25-fold higher concentration (~75 mg/kg/day treatment) of DGJ than the usual dose (3 mg/kg/day treatment), which did not inhibit α-Gal A activity nor increase the tissue Gb3 level (Fig. 7), indicating that the tissue concentration of DGJ is below the inhibitory level at oral dosage. From no further reduction of Gb3 content either in heart or kidney tissue was observed by the treatment with DGJ at higher concentrations, the usual dose (3 mg/kg/day treatment) may be a suitable dose for the ASSC effect in our mouse model.

In conclusion, the Gb3-synthase-overexpressing mouse (TgG3S) shows an increased Gb3 level in its organs, and was useful in generating a mouse line (TgG3S(+/−)M(+/−)/KO) that can be used as an animal model for studying the efficacy of ASSC therapy for Fabry disease.

Funding
Grant-in-Aid for Scientific Research (C) [KAKENHI (20590300)] from Japan Society for the Promotion of Science.

Conflict of interest
None declared.

References

1. Brady, O.R., Gal, A.E., Bradley, R.M., Martensson, E., Warshaw, A.L., and Laster, L. (1967) Enzymatic defect

in Fabry's disease: ceramidetrihexosidase deficiency. *N. Engl. J. Med.* **276**, 1163–1167
2. Desnick, R.J., Ioannou, Y.A., and Eng, C.M. (2001) in *The Metabolic and Molecular Bases of Inherited Disease* (Scriver, C.R., Beaudet, A.L., Sly, W.S., and Valle, D., eds.), pp. 3733–3774, McGraw-Hill, New York
3. Ishii, S., Kase, R., Sakuraba, H., and Suzuki, Y. (1993) Characterization of a mutant α-galactosidase gene product for the late-onset cardiac form of Fabry disease. *Biochem. Biophys. Res. Comm.* **197**, 1585–1589
4. Ishii, S., Chang, H.-H., Kawasaki, K., Yasuda, K., Wu, H.-L., Garman, S.C., and Fan, J.-Q. (2007) Mutant α-galactosidase A enzymes identified in Fabry patients with residual enzyme activity: biochemical characterization and restoration of normal intracellular processing by 1-deoxygalactonojirimycin. *Biochem. J.* **406**, 285–295
5. Hamanaka, R., Shinohara, T., Yano, S., Nakamura, M., Yasuda, A., Yokoyama, S., Fan, J.-Q., Kawasaki, K., Watanabe, M., and Ishii, S. (2008) Rescue of mutant a-galactosidase A in the endoplasmic reticulum by 1-deoxygalactonojirimycin leads to trafficking to lysosomes. *Biochim. Biophys, Acta* **1782**, 408–413
6. Fan, J.-Q., Ishii, S., Asano, N., and Suzuki, Y. (1999) Accelerated transport and maturation of lysosomal α-galactosidase A in Fabry lymphoblasts by an enzyme inhibitor. *Nat. Med.* **5**, 112–115
7. Fan, J.-Q. and Ishii, S. (2003) Cell-based screening of active site specific chaperone for the treatment of Fabry disease. *Methods Enzymol.* **363**, 412–420
8. Fan, J.-Q. and Ishii, S. (2007) Active-site-specific chaperone therapy for Fabry disease: Yin and Yang of enzyme inhibitors. *FEBS J.* **274**, 4962–4971
9. Benjamin, E.R., Flanagan, J.J., Schilling, A., Chang, H.H., Agarwal, L., Katz, E., Wu, X., Pine, C., Wustman, B., Desnick, R.J., Lockhart, D.J., and Valenzano, K.J. (2009) The pharmacological chaperone 1-deoxygalactonojirimycin increases alpha-galactosidase A levels in Fabry patient cell lines. *J. Inherit. Metab. Dis.* **32**, 424–440
10. Ohshima, T., Murray, G.J., Swaim, W.D., Longenecker, G., Quirk, J.M., Cardarelli, C.O., Sugimoto, Y., Pastan, I., Gottesman, M.M., Brady, R.O., and Kulkarni, A.B. (1997) α-Galactosidase A deficient mice: a model of Fabry disease. *Proc. Natl Acad. Sci. USA* **94**, 2540–2544
11. Ioannou, Y.A., Zeidner, K.M., Gordon, R.E., and Desnick, R.J. (2001) Fabry disease: preclinical studies demonstrate the effectiveness of α-galactosidase A replacement in enzyme-deficient mice. *Am. J. Hum. Genet.* **68**, 14–25
12. Ziegler, R.J., Yew, N.S., Li, C., Cherry, M., Berthlette, P., Romanczuk, H., Ioannou, Y.A., Zeidner, K.M., Desnick, R.J., and Cheng, S.H. (1999) Correction of enzymatic and lysosomal storage defects in Fabry mice by adenovirus-mediated gene transfer. *Hum. Gene Ther.* **10**, 1667–1682
13. Takenaka, T., Murray, G.J., Qin, G., Quirk, J.M., Ohshima, T., Qasba, P., Clark, K., Kurkarni, A.B., Brady, R.O., and Medin, J.A. (2000) Long-term enzyme correction and lipid reduction in multiple organs of primary and secondary transplanted Fabry mice receiving transduced bone marrow cells. *Proc. Natl Acad. Sci. USA* **97**, 7515–7520
14. Nakamura, G., Maruyama, H., Ishii, S., Shimotori, M., Kameda, S., Kono, T., Miyazaki, J., Kulkarni, A.B., and Gejyo, F. (2008) Naked plasmid DNA-based alpha-galactosidase A gene transfer partially reduces systemic accumulation of globotriaosylceramide in Fabry mice. *Mol. Biotechnol.* **38**, 109–119
15. Abe, A., Gregoory, S., Lee, L., Killen, P.D., Brady, R.O., Kulkarni, A., and Shayman, J.A. (2000) Reduction of globotriaosylceramide in Fabry disease mice by substrate deprivation. *J. Clin. Invest.* **105**, 1563–1571
16. Ishii, S., Yoshioka, H., Mannen, K., Kulkarni, A.B., and Fan, J.-Q. (2004) Transgenic mouse expressing human mutant α-galactosidase A in an endogenous enzyme deficient background: a biochemical animal model for studying active-site specific chaperone therapy for Fabry disease. *Biochim. Biophys. Acta* **1690**, 250–257
17. Shimmoto, M., Kase, R., Itoh, K., Utsumi, K., Ishii, S., Taya, C., Yonekawa, H., and Sakuraba, H. (1997) Generation and characterization of transgenic mice expressing a human mutant α-galactosidase with an R301Q substitution causing a variant form of Fabry disease. *FEBS Lett.* **417**, 89–91
18. Ishii, S., Chang, H.-H., Yoshioka, H., Shimada, T., Mannen, K., Higuchi, Y., Taguchi, A., and Fan, J.-Q. (2009) Preclinical efficacy and safety of 1-deoxygalactonojirimycin in mice for Fabry disease. *J. Pharmacol. Exp. Ther.* **328**, 723–731
19. Kojima, Y., Fukumoto, S., Furukawa, K., Okajima, T., Wiels, J., Yokoyama, K., Suzuki, Y., Urano, T., Ohta, M., and Furukawa, K. (2000) Molecular cloning of globotriaosylceramide/CD77 synthase, a glycosyltransferase that initiates the synthesis of globo series glycosphingolipids. *J. Biol. Chem.* **275**, 15152–15156
20. Niwa, H., Yamamura, K., and Miyazaki, J. (1991) Efficient selection for high-expression transfectants with a novel eukaryotic vector. *Gene* **108**, 193–200
21. Matsuda, J., Suzuki, O., Oshima, A., Yamamoto, Y., Noguchi, A., Takimoto, K., Itoh, M., Matsuzaki, Y., Yasuda, Y., Ogawa, S., Sakata, Y., Nanba, E., Higaki, K., Ogawa, Y., Tominaga, L., Ohno, K., Iwasaki, H., Watanabe, H., Brady, R.O., and Suzuki, Y. (2003) Chemical chaperone therapy for brain pathology in G(M1)-gangliosidosis. *Proc. Natl Acad. Sci. USA* **100**, 15912–15917
22. Ishii, S., Katsumura, T., Shiozuka, C., Ooyauchi, K., Kawasaki, K., Takigawa, S., Fukushima, T., Tokuji, Y., Kinoshita, M., Ohnishi, M., Kawahara, M., and Ohba, K. (2008) Anti-inflammatory effect of buckwheat sprout in lipopolysaccharide-activated human colon cancer cells and mice. *Biosci. Biotechnol. Biochem.* **72**, 3148–3157
23. Shin, I.-S., Nishikawa, K., Maruyama, H., and Ishii, S. (2006) Histidine-tagged Shiga toxin B subunit binding assay: simple and specific determination of Gb3 content in mammalian cells. *Chem. Pharm. Bull.* **54**, 522–527
24. Yano, S., Kashima, K., Daa, T., Urabe, S., Tsuji, K., Nakayama, I., and Yokoyama, S. (2003) An antigen retrieval method using an alkaline solution allows immunoelectron microscopic identification of secretory granules in conventional epoxy-embedded tissue sections. *J. Histochem. Cytochem.* **51**, 199–204
25. Jacewicz, M., Clausen, H., Nudelman, E., Donohue-Rolfe, A., and Keusch, G.T. (1986) Pathogenesis of shigella diarrhea. XI. Isolation of a shigella toxin-binding glycolipid from rabbit jejunum and HeLa cells and its identification as globotriaosylceramide. *J. Exp. Med.* **163**, 1391–1404
26. Lingwood, C.A., Law, H., Richardson, S., Petric, M., Brunton, J.L., De Grandis, S., and Karmali, M. (1987) Glycolipid binding of purified and recombinant Escherichia coli produced verotoxin *in vitro*. *J. Biol. Chem.* **262**, 8834–8839

27. McCluer, R.H. and Gross, S.K. (1985) Biosynthesis of neutral glycosphingolipids in kidney slices from male and female mice. *J. Lipid Res.* **26**, 593–599
28. Ohshima, T., Schiffmann, R., Murray, G.J., Kopp, J., Quirk, J.M., Stahl, S., Chan, C.C., Zerfas, P., Tao-Cheng, J.H., Ward, J.M., Brady, R.O., and Kulkarni, A.B. (1999) Aging accentuates and bone marrow transplantation ameliorates metabolic defects in Fabry disease mice. *Proc. Natl Acad. Sci. USA* **96**, 6423–6427
29. Khanna, R., Soska, R., Lun, Y., Feng, J., Franscella, M., Young, B., Brignol, N., Pellegrino, L., Sitaraman, S., Desnick, R.J., Benjamin, E.R., Lockhart, D.J., and Valenzano, K.J. (2010) The pharmacological chaperone 1-deoxygalactonojirimycin reduces tissue globotriaosylceramide levels in a mouse model of Fabry disease. *Mol. Ther.* **18**, 23–33
30. Asano, N., Ishii, S., Kizu, H., Ikeda, K., Yasuda, K., Kato, A., Martin, O.R., and Fan, J.-Q. (2000) *In vitro* inhibition and intracellular enhancement of lysosomal α-galactosidase A activity in Fabry lymphoblasts by 1-deoxygalactonojirimycin and its derivatives. *Eur. J. Biochem.* **267**, 4179–4186

Diabetes-accelerated memory dysfunction via cerebrovascular inflammation and Aβ deposition in an Alzheimer mouse model with diabetes

Shuko Takeda[a,b], Naoyuki Sato[a,b], Kozue Uchio-Yamada[c], Kyoko Sawada[c], Takanori Kunieda[c], Daisuke Takeuchi[a,b], Hitomi Kurinami[a,b], Mitsuru Shinohara[a,b], Hiromi Rakugi[b], and Ryuichi Morishita[a,1]

Departments of [a]Clinical Gene Therapy and [b]Geriatric Medicine, Graduate School of Medicine, Osaka University, Osaka 565-0871, Japan; and [c]Laboratory of Experimental Animal Models, National Institute of Biomedical Innovation, Osaka 567-0085, Japan

Edited by Thomas C. Südhof, Stanford University School of Medicine, Palo Alto, CA, and approved February 18, 2010 (received for review January 19, 2010)

Recent epidemiological studies suggest that diabetes mellitus is a strong risk factor for Alzheimer disease. However, the underlying mechanisms remain largely unknown. In this study, to investigate the pathophysiological interaction between these diseases, we generated animal models that reflect the pathologic conditions of both diseases. We crossed Alzheimer transgenic mice (APP23) with two types of diabetic mice (*ob/ob* and NSY mice), and analyzed their metabolic and brain pathology. The onset of diabetes exacerbated Alzheimer-like cognitive dysfunction without an increase in brain amyloid-β burden in double-mutant (APP$^+$-*ob/ob*) mice. Notably, APP$^+$-*ob/ob* mice showed cerebrovascular inflammation and severe amyloid angiopathy. Conversely, the cross-bred mice showed an accelerated diabetic phenotype compared with *ob/ob* mice, suggesting that Alzheimer amyloid pathology could aggravate diabetes. Similarly, APP$^+$-NSY fusion mice showed more severe glucose intolerance compared with diabetic NSY mice. Furthermore, high-fat diet feeding induced severe memory deficits in APP$^+$-NSY mice without an increase in brain amyloid-β load. Here, we created Alzheimer mouse models with early onset of cognitive dysfunction. Cerebrovascular changes and alteration in brain insulin signaling might play a pivotal role in this relationship. These findings could provide insights into this intensely debated association.

β-amyloid | insulin

The incidences of Alzheimer disease (AD) and diabetes mellitus (DM) are increasing at an alarming rate and have become major public health concerns (1, 2). Interestingly, numerous epidemiological studies demonstrated that diabetic patients have a significantly higher risk of developing AD, independent of the risk for vascular dementia (2, 3). These findings raise the possibility that DM may affect fundamental AD pathogenesis. A neuropathological hallmark of AD is β-amyloid peptide (Aβ) accumulation in the brain (4). Of importance, recent data showed a clear relationship between insulin and Aβ metabolism (5–7). For example, insulin increased the extracellular Aβ level by modulating γ-secretase activity (6), or by increasing its secretion from neurons (5). Insulin-degrading enzyme, a major Aβ-degrading enzyme, might be competitively inhibited by insulin, resulting in decreased Aβ degradation (7). In addition, the brain insulin-degrading enzyme level was decreased in a hyperinsulinemic Alzheimer animal model (8). Nevertheless, unexpectedly, there is no evidence that the typical pathological hallmarks of AD, including amyloid plaque, are increased in the brain of diabetic patients (9, 10). Thus, DM could affect the pathogenesis of AD through other mechanisms than modulating Aβ metabolism. One possible mechanism is cerebrovascular alteration, a common pathological change in DM and AD. Accumulating evidence suggests the importance of Aβ-induced cerebrovascular dysfunction in AD (11). Moreover, cerebrovascular disease is a major complication of DM. Vascular inflammation or oxidative stress mediated by the receptor for advanced glycation end products (RAGE) has been shown to be a possible mechanism for vascular dysfunction in diabetes (12). RAGE also functions as a putative Aβ receptor and plays a significant role in AD (13, 14).

To further elucidate the underlying mechanisms linking AD and DM, we generated animal models that reflect the pathologic conditions of both diseases. We crossed APP23 transgenic mice, a well established animal model for AD, which express human-type amyloid precursor protein (APP) derived from a large Swedish family with early-onset AD (15), with leptin-deficient *ob/ob* mice or polygenic NSY mice (16) as a model for DM. Our present results provide insights into the mechanisms underlying the pathological relationship between AD and DM.

Results

Metabolic Features of APP$^+$-*ob/ob* Mice. To evaluate the impact of diabetic symptoms on the pathophysiology of AD, we generated an animal model by crossbreeding APP23 mice and diabetic ob/ob mice. APP$^+$-*ob/ob* mice showed early-onset obesity compared with original APP$^+$ mice (Fig. 1 *A* and *B*). In addition, APP$^+$-*ob/ob* mice showed severe hyperglycemia (Fig. 1*C*), hyperinsulinemia (Fig. 1*D*), glucose intolerance on glucose tolerance test (GTT) (Fig. 1*E*), and hyperlipidemia (Fig. S1) compared with APP$^+$ mice at 8 weeks. Of importance, the diabetic phenotype was markedly more severe in APP$^+$-*ob/ob* mice than in original *ob/ob* mice (Fig. 1 *C–G*), although APP$^+$-*ob/ob* mice were slightly leaner than *ob/ob* mice (Fig. 1*B*). APP$^+$-*ob/ob* mice showed more marked glucose intolerance than *ob/ob* mice in GTT (Fig. 1*E*). Insulin sensitivity measured by the reduction in blood glucose after insulin administration was markedly reduced in APP$^+$-*ob/ob* mice compared with *ob/ob* mice (Fig. 1*F*). There was no significant difference in insulin sensitivity between APP$^+$ and WT mice (Fig. 1*G*). We studied insulin signaling (Akt phosphorylation) in liver and muscle to estimate the contribution of these insulin-sensitive peripheral organs to the aggravation of insulin resistance in APP$^+$-*ob/ob* mice. In a reflection of their severe insulin resistance, APP$^+$-*ob/ob* mice showed suppression of insulin-stimulated Akt phosphorylation (Ser473) compared with *ob/ob* mice in these organs, without alterations in total Akt concentration (Fig. 1 *H* and *I*). No significant difference was observed between APP$^+$ and WT mice (Fig. 1 *H* and *I*). APP$^+$-*ob/ob* mice and *ob/ob* mice showed no difference in daily food intake (Fig. 1*J*) and basal activity (Fig.

Author contributions: S.T., N.S., K.U.-Y., K.S., T.K., D.T., H.K., M.S., H.R., and R.M. designed research; S.T., K.U.-Y., K.S., and T.K. performed research; S.T., N.S., K.U.-Y., K.S., T.K., M.S., H.R., and R.M. analyzed data; and S.T., N.S., and R.M. wrote the paper.

The authors declare no conflict of interest.

This article is a PNAS Direct Submission.

See Commentary article on page 6557.

[1]To whom correspondence should be addressed. E-mail: morishit@cgt.med.osaka-u.ac.jp.

This article contains supporting information online at www.pnas.org/cgi/content/full/1000645107/DCSupplemental.